J. Phase Equilib. Diffus. (2017) 38:353–368
DOI 10.1007/s11669-017-0570-7

TCHEA1: A Thermodynamic Database Not Limited for "High Entropy" Alloys

Huahai Mao[1,2] · Hai-Lin Chen[2] · Qing Chen[2]

Submitted: 24 April 2017 / in revised form: 1 June 2017 / Published online: 5 July 2017

Abstract In this paper we report a thermodynamic database which was developed by using the CALPHAD approach. The TCHEA1 database includes 15 chemical elements (Al, Co, Cr, Cu, Fe, Hf, Mn, Mo, Nb, Ni, Ta, Ti, V, W and Zr). It is suitable for the study of Bcc and Fcc HEA systems. The database is constructed based on the thermodynamic assessment of all binary systems and many key ternary systems where almost all possible metastable and stable phases are considered. It is extensively demonstrated in the present work that TCHEA1 gives satisfactory prediction on the phase equilibria in various HEA systems (quaternary to ennead) and wide temperature ranges (liquidus to subsolidus). Thermodynamic stability calculations of simple solid solutions (Bcc and Fcc) and intermetallics (sigma, Laves, μ-phase etc.) are validated against the available experimental information in as-cast or as-annealed state. Such CALPHAD database focusing on the modelling of Gibbs energy rather than entropy makes reliable predictions of thermodynamic equilibrium and phase transformation, no matter whether the alloy/system has high entropy or not. Cases with miscibility gap in liquid and solid solutions and second-order phase transition at low temperatures are demonstrated. With the volume data included, TCHEA1 is capable to predict the density and thermal expansion coefficient of HEAs as well. This thermodynamic database is also applicable in process simulations when used together with compatible kinetic databases.

Keywords CALPHAD · computational thermodynamics · high-entropy alloys · phase diagram · solid solution

1 Introduction

High entropy alloys (HEAs) have gained ever-increasing attention from academia and industries since the concept was firstly proposed in 2004.[1,2] The concept of HEA opens new areas in materials science and engineering. It stimulates the exploration of new alloy systems from the traditional small corner composition regions to the vast uncharted central fields in the multi-dimensional composition space. This paradigm shift provides us unlimited opportunities to design and develop new materials through various combinations of chemical elements. As the number of possible combinations is immense, even a small fraction of it is still unbelievably large. This tremendous potential has driven an explosive increase of interest in HEAs in recent years as reviewed in the recent publications.[3–5] Obviously the exploration of new HEAs in the multi-dimensional composition space cannot rely on Edisonian approach. It requires a more efficient and systematical strategy. To meet the challenges, computational methods are indispensable. Different computational approaches, ranging from empirical rules[6,7] to semi-empirical CALPHAD method,[8–12] and to theoretical first principles method,[13,14] have been applied for screening of HEAs. For example, many empirical rules in terms of mixing enthalpy, configurational entropy, atomic size mismatch, valence electron concentration and their various combinations, have been proposed and tested to explore potential

✉ Huahai Mao
huahai@kth.se

[1] Materials Science and Engineering, KTH Royal Institute of Technology, Brinellvägen 23, 10044 Stockholm, Sweden

[2] Thermo-Calc Software AB, Råsundavägen 18A, 16967 Solna, Sweden

HEAs of simple solid solutions. This method works well in some particular HEA systems where intermetallics are unstable. Nevertheless, it is oversimplified to study the stability of some particular phases without considering the total Gibbs energy minimization of the whole system at various temperatures. On the other hand, the first principles calculations are too computationally expensive. It is not feasible to study the phase stability at finite temperatures of multi-component HEA systems. The semi-empirical CALPHAD approach is the optimal method for this purpose.

The calculation of phase diagrams (CALPHAD) method has been widely and successfully employed in materials science and engineering for decades.[15,16] With the CALPHAD approach, the integral Gibbs energy, including enthalpy or entropy, of each phase is thermodynamically modeled and evaluated as a function of temperature, pressure, and composition in low-order systems. During the thermodynamic assessment the phase diagram and thermodynamic property information are coupled. Thermodynamic equilibria are determined by the Gibbs energy minimization of the whole system including all possible phases. By using a CALPHAD computational tool, for example Thermo-Calc,[17] together with a self-consistent thermodynamic database, both thermodynamic properties and phase equilibria in the binary and ternary as well as multicomponent systems can be calculated on the basis of Gibbsian thermodynamics.

In this paper we report a special thermodynamic database, TCHEA1, for the application in HEA systems. The credibility of a CALPHAD calculation is solely dependent on the suitability and quality of the thermodynamic database used. For the study of conventional single principal element alloys it is good enough for a database if the thermodynamic descriptions mainly focus on the ternary systems containing the major component, and the thermodynamic descriptions may not be complete for a whole system but limited to the major component rich corner, and irrelevant phases to the targeted type of alloys are deliberately excluded. However, these databases for conventional alloys are apparently not adequate for making phase stability predictions for HEA systems where all ternary systems are in theory equally important. The new thermodynamic database TCHEA1 has been developed without the simplifications and omissions pertinent to conventional databases. In this database, all binary and many key ternary systems have been assessed. Since its debut about 2 years ago, TCHEA1 has been applied by many groups interested in HEAs to interpret the experimental phase formation and to explore new alloys and new compositions.[18–23]

In this paper, an overview about this thermodynamic database is given firstly in section 2. Followed in section 3 where selected thermodynamic models applied for the important phases namely Bcc, Fcc, sigma and Laves phases are illustrated. The main body of this paper is section 4, where extensive validation cases using TCHEA1 are demonstrated in various HEA systems over wide temperature ranges. Thereafter, some extended discussions on the application area of this database are given in section 5. In section 6 some concluding remarks and future works are highlighted finally.

2 Database Overview

TCHEA1 is a thermodynamic database developed especially for high entropy alloys or multi-principal element alloys. It is developed in a CALPHAD spirit based on the critical evaluation of all the binary systems and many ternary systems. A hybrid approach of experiments, first-principals calculations and CALPHAD modeling had been used to obtain reliable thermodynamic descriptions of the Bcc and Fcc solutions. That enables predictions to be made for multi-component alloy systems, especially for HEAs. The database has been developed in a 15-element framework: Al, Co, Cr, Cu, Fe, Hf, Mn, Mo, Nb, Ni, Ta, Ti, V, W and Zr. All the 105 binary systems in this 15-element framework have been assessed to their full range of composition and temperature. It can be calculated with the Binary Module in Thermo-Calc. In total, 200 ternaries have been assessed, and 104 of them to their full range of composition and temperature. They can be calculated with the Ternary Module in Thermo-Calc.

TCHEA1 contains nearly all stable phases in all assessed binary systems and most ternary systems. In total, 163 solution and intermetallic phases are modelled. The complete list of phases is available on the website of Thermo-Calc (www.thermocalc.com). The database can be used to calculate various phase diagrams and property diagrams in the assessed systems and higher-order systems. The extrapolation to higher-order systems helps to understand the phase equilibria in HEAs, so as to predict the phase formation, phase fractions and phase compositions or to calculate the driving force of forming a new phase. The database can also be used for predicting solidification behaviour of HEAs with the Scheil_Gulliver module in Thermo-Calc. All available molar volume data and thermal expansion data have been assessed or estimated for most of the phases.

3 Thermodynamic Models

A complete database for HEAs in principle should include and well describe all the stable phases. Even if the formation of alloys of simple solid solutions is desired, the

competitions from the intermetallic phases must be considered. Most stable solid phases are modelled in each assessed binary and ternary system, unless in the case of lacking of experimental evidences or data. Appropriate thermodynamic models are used for different types of phases.

3.1 Solution Phases

For a n-component substitutional solution phase ($\emptyset$), such as liquid, Fcc_A1, Bcc_A2, or Hcp_A3, its Gibbs energy $G^{\emptyset}$ is described as a function of the composition (x_i) and temperature (T) as:

$$G^{\emptyset} = \sum_{i}^{n} x_i G_i^{\emptyset} + RT \cdot \sum_{i}^{n} x_i \ln(x_i) + \sum_{i=1}^{n-1} \sum_{j=i+1}^{n} x_i x_j L_{ij} + \sum_{i=1}^{n-2} \sum_{j=i+1}^{n-1} \sum_{k=j+1}^{n} x_i x_j x_k L_{ijk} \quad \text{(Eq 1)}$$

The Gibbs energy for each pure element i in the form of $\emptyset$, $G_i^{\emptyset}$, is taken from the SGTE PURE5 database. L_{ij} and L_{ijk} are the interaction parameters assessed, respectively, in each individual binary and ternary system. The binary interaction parameters L_{ij} are expanded by the Redlish–Kister polynomial $L_{ij} = {}^0L + {}^1L(x_i - x_j) + {}^2L(x_i - x_j)^2 + \cdots$, the parameters ${}^0L$, ${}^1L$, ${}^2L$, and so on can be temperature dependent. The solution is usually called regular if L_{ij} is represented solely by the ${}^0L$ term, i.e., when L_{ij} is composition-independent. The ternary interaction parameters are expressed by $L_{ijk} = v_i \cdot {}^iL_{ijk} + v_j \cdot {}^jL_{ijk} + v_k \cdot {}^kL_{ijk}$, where $v_i = x_i + (1 - x_i - x_j - x_k)/3$, $v_j = x_j + (1 - x_i - x_j - x_k)/3$, $v_k = y_k + (1 - x_i - x_j - x_k)/3$. This expression of composition-dependent provides a symmetrical extension into higher order systems. It should be noted that the magnetic contribution to the Gibbs energy is also considered in the database. The expression is not given here in order to save space.

3.2 Sublattice Model

In crystalline solids, different atoms often preferably occupy different types of sites, which are known as Wyckoff sites. In CALPHAD, the concept of "sublattice" was invented to distinguish the sites and describe the site occupancies in a more physically meaningful way.[15] Different from the one-sublattice substitutional model, models with two or more sublattices are referred to as sublattice models.[1] Simplifications are often necessary to make a model applicable, by coupling several Wyckoff sites with similar occupancies as one sublattice. The number of sublattices depends on the crystallographic and compositional complexity. In CALPHAD modeling, sublattice models are the most frequently used ones.

In TCHEA1, most sublattice models consist of only 2SLs and 3SLs in order to assure the efficiency in both the development and the calculation. For instance, the Laves phases, C14, C15 and C36, respectively, are modeled with a 2SL model (A, B, …)$_2$(A, B, …)$_1$. Assuming that m constituents are on the first lattice and n constituents on the second one, the Gibbs energy can be expressed as below,

$$\begin{aligned} G^{\emptyset} = {} & \sum_{i=1}^{m} \sum_{j=1}^{n} y_i^{(1)} y_j^{(2)} G_{i:j}^{\emptyset} + RT \\ & \cdot \left(2 \cdot \sum_{i}^{m} y_i^{(1)} \ln(y_i^{(1)}) + \sum_{i}^{n} y_i^{(2)} \ln\left(y_i^{(2)}\right) \right) \\ & + \sum_{i=1}^{m-1} \sum_{j=i+1}^{m} \sum_{k}^{n} y_i^{(1)} y_j^{(1)} y_k^{(2)} L_{ij:k} \\ & + \sum_{i=1}^{n-1} \sum_{j=i+1}^{n} \sum_{k}^{m} y_k^{(1)} y_i^{(2)} y_j^{(2)} L_{k:ij} \\ & + \sum_{i=1}^{m-1} \sum_{j=i+1}^{m} \sum_{k=1}^{n} \sum_{l=k+1}^{n-1} y_i^{(1)} y_j^{(1)} y_k^{(2)} y_l^{(2)} L_{ij:kl} \end{aligned} \quad \text{(Eq 2)}$$

3.3 Partitioning Model

In many alloy systems, the common ordered structures $L1_2$ and B2 exist. $L1_2$ can be regarded as an ordered structure of Fcc_A1 and B2 as an ordered structure of Bcc_A2. In order to describe the potential second-order transition between an ordered structure and its disordered counterpart, the ordered and disordered structures have to be described with a single continuous Gibbs energy description[24,25] using the so-called partitioning model,

$$G_m = G_m^{dis}(x_i) + G_m^{ord}\left(y_i^s\right) - G_m^{ord}(x_i) \quad \text{(Eq 3)}$$

The first term corresponds to the Gibbs energy of the disordered structure, which can be independently assessed on the experimental information of the corresponding disordered phase, and it is described with the substitutional model. The second and the third terms are the contributions from the ordering parameters calculated by using the site fractions y_i^s and the mole fractions x_i respectively. The difference between the second and the third term is the Gibbs energy of ordering. When the phase is fully

[1] It should be noted that nowadays the models for substitutional solid solutions often have an additional vacancy sublattice accommodating possible interstitial elements. Actually, when the solubility of interstitial elements is considered, such additional vacancy sublattices may have to be added for phases that are already described with sublattice models as well.

disordered, the fractions of each constituent on each site are equal and thus equal to the mole concentration, i.e., $y_i^s = x_i$, and the second and the third terms cancel out each other so that the total energy is identical to that of the disordered part.

Note that there may be several possible composition sets for the phases named Fcc_L1$_2$ and Bcc_B2 designated by #1, #2, and so on (e.g., Fcc_L1$_2$#1 and Fcc_L1$_2$#2), due to the co-existence of disordered and ordered structures or the presence of miscibility gap. The #n suffix (where n is an integer) is generated dynamically by Thermo-Calc when using global minimization and therefore the identification of the phases should be determined from their site occupations.

3.4 Sigma Phase

The sigma phase is described with the so-called "non-disorder partitioning model".

$$G_m = G_m^{dis}(x_i) + G_m^{ord}\left(y_i^s\right) \quad \text{(Eq 4)}$$

The imaginary disordered sigma phase is described with a single sublattice, and its energy, $G_m^{dis}(x_i)$, is given in a similar way as that for the solution phases described by Eq 1.

Even though the ordered sigma phase has 5 Wyckoff sites, it is described with a 3SL model, (A, B, …)$_{10}$ (A, B, …)$_4$(A, B, …)$_{16}$, for the sake of simplification. The first lattice corresponds to a combination of the 2a and 8i$_2$ sites, the second to the 4f site, and the third to the combination of 8i$_1$ and 8j sites.[26] The combinations were made by considering the similarity in the experimental site occupancies in most sigma phases observed in different systems.[26] The second term, $G_m^{ord}(y_i^s)$, is the contribution from the ordering parameters to the Gibbs energy. Due to the lack of a third term as in Eq 3, the sigma phase can never be fully disordered, which is reasonable and is intended since sigma is in principle more or less an ordered phase.

All the lattice stability parameters for pure elements and the binary interaction parameters, together with some ternary interaction parameters, of the disordered part are assessed first. Since there is only one sublattice, the number of parameters is small. These parameters provide a good approximation of the energy for the actual sigma phase, so that it is not necessary to assess the ordering parameters for all the unstable endmember. The important endmembers can be assessed in individual systems where sigma is stable. With such a partitioning treatment, the number of parameters that need to be assessed was significantly reduced.

The non-disorder partitioning model was also employed to describe the Fe_7W_6-type μ-phase.

4 Validation Examples

4.1 Typical Bcc Systems

Typical Bcc HEA systems are made of elements that are stable in the Bcc structure at ambient pressure. Special interests are paid on refractory elements, such as Mo, Nb, Ta, Ti, V, W and Zr etc., as well as the non-Bcc Al element. Even though Al is of the Fcc structure, it shows large solubilities in many Bcc metals and may stabilize the ordered B2 structure.

Figure 1(a) shows the calculated mole fraction of equilibrium phases in the equiatomic NbTaTiV quaternary

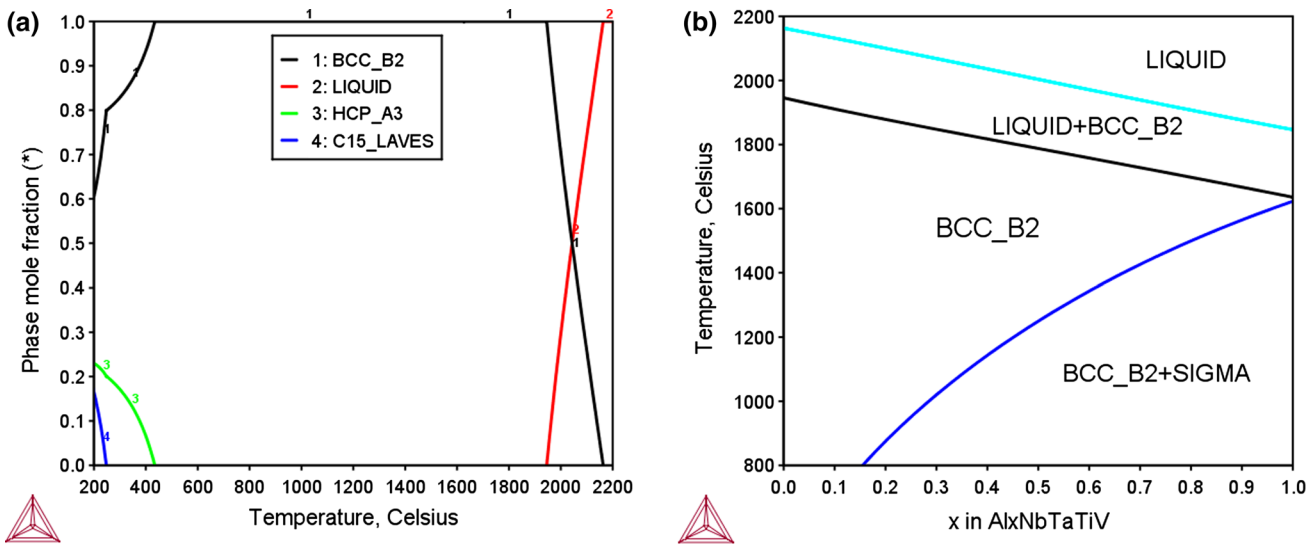

Fig. 1 (a) Calculated mole fraction of equilibrium phases in the equiatomic NbTaTiV quaternary alloy. (b) Predicted phase equilibria in the isopleth for the series of the Al$_x$NbTaTiV quinary alloys, where x = 0-1 represents moles of atoms of the element Al

alloy at various temperatures. The disordered Bcc phase (labeled as BCC_B2 in the figure) is the only crystalline phase from the liquidus temperature down to 434 °C, which suggests that the as-cast alloy would be of the single Bcc phase even if the solidification severely deviates from the equilibrium conditions. According to Fig. 1(b), with an Al addition in the range of 0-1, disordered Bcc remains as the only solid phase that forms via solidification, which agrees with the experimental observations in as-cast Al_x-$Nb_1Ta_1Ti_1V_1$ ($0 < x < 1$) alloys.[27] It should be noted that the Al addition noticeably stabilizes the sigma phase and makes it possible for the sigma phase to form during non-equilibrium solidification at high Al contents.

The $Nb_1Ti_1V_1Zr_1$ alloy was experimentally investigated in both as-cast and heat treated states by Senkov et al.[28] The heat treatment had been performed by homogenizing the as-cast alloys at 1200 °C, followed by slow cooling down to room temperature at the rate of −10 °C/min. The XRD pattern indicates a single Bcc crystal structure. However, the SEM backscatter electron images (BEI) of the homogenized alloy clearly showed some spots about of 3-6 vol.% homogeneously dispersed inside the matrix, but the as-cast alloy was spot-free. The EBSD/EDS analyses evidenced that these spots are depleted of V and enriched in Zr. This can be explained by an incomplete decomposition of the Bcc phase below 723 °C during the slow cooling, as predicted by the equilibrium calculation in Fig. 2 where the primary disordered BCC_B2 decomposes into two phases (BCC_B2 + BCC_B2#2) at low temperatures. The calculation corroborates that Bcc would be the only phase that forms during the solidification and the single phase state remains until the decomposition. The compositions of the two Bcc phases are calculated at 627 °C to be $Nb_{17.1}Ti_{30.1}V_{15.1}Zr_{37.7}$ (at.%, BCC_B2#2) and $Nb_{33.4}Ti_{19.6}V_{35.5}Zr_{11.5}$ (at.%, BCC_B2). The former composition corresponds to the precipitates while the latter to the matrix phase.

Zhang et al.[30] studied the $Mo_1Nb_1Ti_1V_xZr_1$ (x = 0, 0.25, 0.50, 0.75 and 1.00) alloys using high vacuum and suction cast into the water-cooled copper mold. In the as-cast alloys with different amounts of the V addition, XRD exhibited reflections of only a Bcc structure, but overlapping peaks were present in the patterns, which implied that the Bcc phase separation may exist in these alloys. In our calculation (see Fig. 3), not only the formation of the primary Bcc (labeled as BCC_B2 in the figure) during the solidification but also the Bcc phase separation at low temperatures are predicted. The phase stability especially at low temperatures of the $Mo_1Nb_1Ti_1Zr_1$ quaternary HEA (without the V addition) is discussed in the following Fig. 4. It can be seen that the disordered Bcc (labeled as BCC_B2 in the figure) is the only phase crystalizes directly from the liquid. It agrees well with the observed single Bcc structure in the as-cast sample. Moreover, the calculation predicts the miscibility gap of this phase below 1161 °C.

The equiatomic MoNbTiZr solid solution decomposes into almost equal-mole-fraction of two Bcc phases (BCC_B2 & BCC_B2#3 in the figure), implying probable spinodal decomposition at low temperatures. At even lower temperatures (T < 534 °C) down to room temperature, one Bcc phase (i.e., BCC_B2#3) transforms into Hcp phase. The low temperature phase separation was confirmed by the experiment.[30] It is desired to have more advanced experimental technique to verify the spinodal

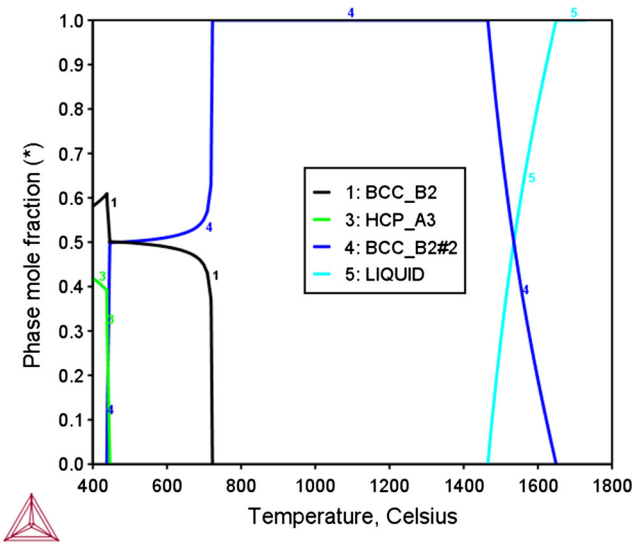

Fig. 2 Calculated mole fraction of equilibrium phases at various temperatures in the NbTiVZr quaternary alloy with equiatomic ratio

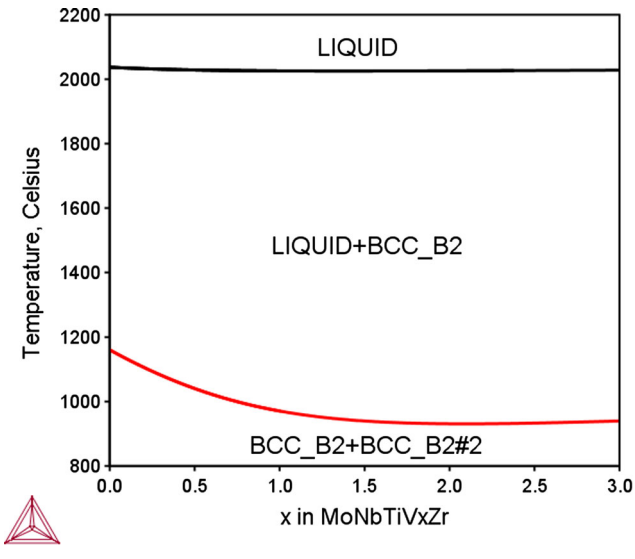

Fig. 3 Predicted phase equilibria in the isopleth for the series of the $MoNbTiV_xZr$ quinary alloys, where x = 0-1 represents moles of atoms of the element V

decomposition mechanism and the possible martensitic phase transformation from Fcc to Hcp in the $Mo_1Nb_1Ti_1Zr_1$ HEA alloy.

Very recently Qiu et al.[31] studied the lightweight single-phase $Al_1Cr_1Ti_1V_1$ alloy. A simple single-phase microstructure was revealed in the as-cast alloy via conventional and scanning transmission electron microscopy. Characterization was supported by atom probe tomography and x-ray diffraction. The unique atomic locations in the alloy verified the crystal structure is the ordered Bcc i.e., B2 structure. Using TCHEA1 database the primary phase precipitating from the $Al_1Cr_1Ti_1V_1$ melt is predicted being the disordered A2 phase (see Fig. 5, the BCC_B2#1 phase). It transfers to the ordered B2 phase (labeled as BCC_B2#2 in the figure) around 692 °C (second-order phase transformation). Around 527 °C the B2 phase starts decomposing into some intermetallic phases. The observation of B2 phase in the as-cast alloy can be expected as a result of the second-order phase transformation from the coherent primary A2 phase. However, due to the sluggish kinetic at low temperatures and incoherency between Bcc matrix and intermetallic precipitates no second phase was observed in the as-cast alloy. The density of the alloy produced in Ref 31 was measured to be 5.06 g/cm^3, verifies our calculated value of 5.04 g/cm^3.

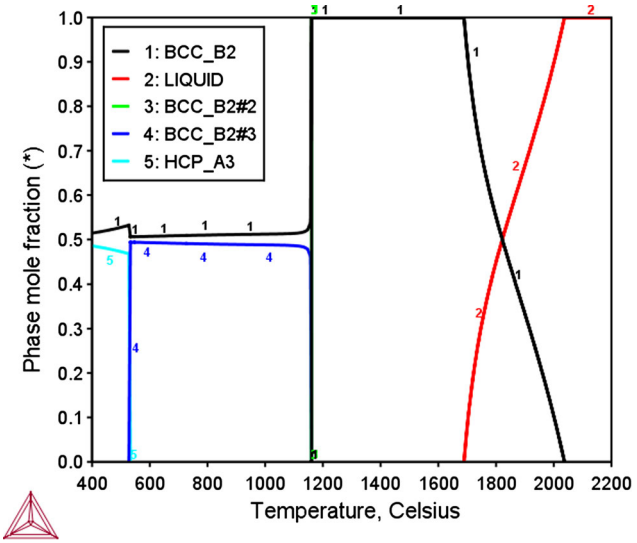

Fig. 4 Calculated mole fraction of equilibrium phases at various temperatures in the MoNbTiZr quaternary alloy with equiatomic ratio

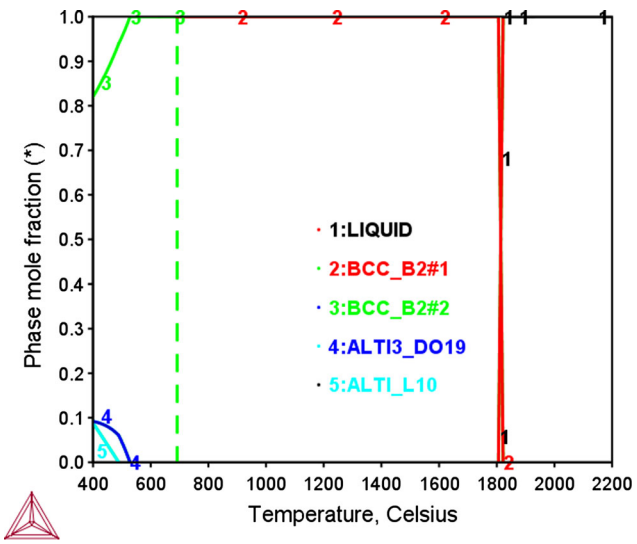

Fig. 5 Calculated mole fraction of equilibrium phases at various temperatures in the AlCrTiV quaternary alloy with equiatomic ratio

4.2 Typical Fcc Systems

Many frequently investigated Fcc-type HEAs are based on the Co-Cr-Cu-Fe-Ni system and its subsystems. Single Fcc structure was observed in the as-cast $Co_1Cr_1Fe_1Ni_1$ alloy,[32] and the alloy annealed at 850 °C for 24 h[33] and 750 °C for 800 h.[34] The stability of the Fcc phase in the $Co_1Cr_1Fe_1Ni_1$ alloy was predicted by the TCHEA1 database (see Fig. 6, the FCC_L12 denotes the disordered Fcc phase).

As-cast $Co_1Cr_1Cu_1Fe_1Ni_1$ HEA alloys were fabricated by Yeh et al.[1,35] with splat quenching at a cooling rate around 10^3-10^4 °C/s and by Tong et al.[36] using directional solidification in the cold copper hearth with a cooling rate about 1-10 °C/s. Only the Fcc structure was detected in the as-cast alloys in these experimental investigations, similar to that in as-cast $Co_1Cr_1Fe_1Ni_1$ alloys. The Cu addition, however, caused a phase separation. The typical dendritic microstructure consists of Cu-lean Fcc dendrites and Cu-

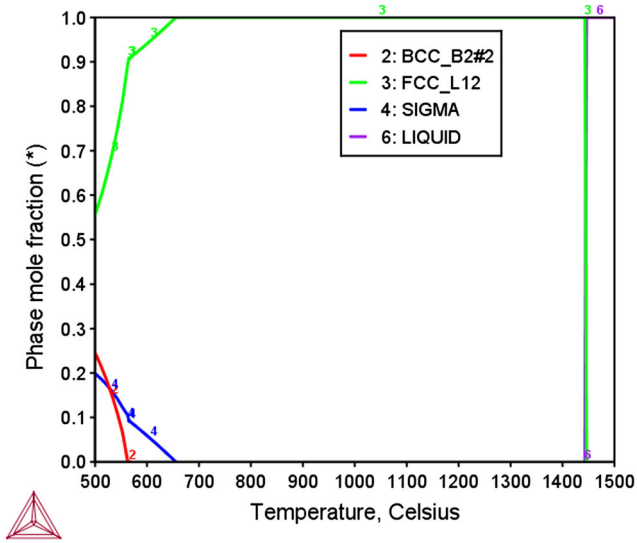

Fig. 6 Calculated mole fraction of equilibrium phases at various temperatures in the CoCrFeNi equiatomic alloy

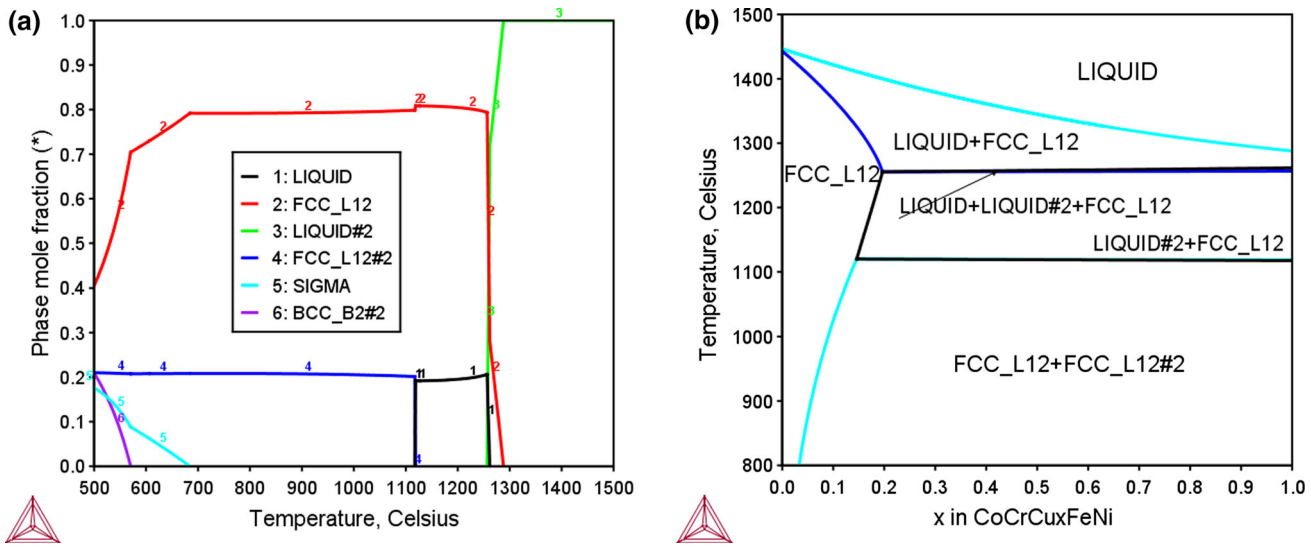

Fig. 7 (a) Calculated mole fraction of equilibrium phases at various temperatures in the CoCrCuFeNi equiatomic alloy. (b) Predicted phase equilibria in the isopleth for the series of the $CoCrCu_xFeNi$ quinary alloys, where x = 0-1 represents moles of Cu atoms

rich Fcc interdendritic region.[1,35,36] Figure 7(a) shows the calculated mole fraction of equilibrium phases at various temperatures in the $Co_1Cr_1Cu_1Fe_1Ni_1$ alloy. It can be seen that both the primary (labeled as FCC_L12) and the secondary (FCC_L12#2) phases are of Fcc structure. Results at 927 °C give that the primary Fcc phase (i.e., the dendrites) has a composition of $Co_{25.0}Cr_{25.1}Cu_{1.5}Fe_{25.0}Ni_{23.4}$ (at.%), while the secondary Fcc phase (i.e., the interdendrite region) has a composition of $Co_{0.8}Cr_{0.3}Cu_{91.0}Fe_{1.0}Ni_{6.9}$ (at.%). The former is nearly Co-Cr-Fe-Ni equiatomic and almost free of Cu while the latter is absolutely Cu-dominating, so the immiscibility was fully caused by Cu.

Hsu et al.[32] studied the impact of the Cu content on the $Co_1Cr_1Cu_xFe_1Ni_1$ (x = 0, 0.5 and 1) alloys and the phase separation was observed at x = 0.5 and 1. With the aid of the calculated isopleth in Fig. 7(b), we know that the phase separation could occur at much lower Cu contents. Even though a single Fcc phase can be attained at x = 0.196 at 1256 °C, it would probably decompose at lower temperatures.

The stability of the Fcc phase at low temperatures was studied by Singh and Subramaniam.[33] The as-cast $Co_1Cu_1Fe_1Ni_1$ alloy was annealed for 24 h at 850 °C. It was revealed by XRD and SEM that there were two Fcc phases. The major Fcc is Cu-poor while the minor Fcc is Cu-rich. At 850 °C our calculation predicts FCC_L12 (82.5 vol.%) in equilibrium with FCC_L12#2 (17.5 vol.%). Their compositions are: $Co_{29.9}Cu_{11.9}Fe_{29.9}Ni_{28.3}$ and $Cu_{88.5}Co_{1.3}Fe_{1.1}Ni_{9.2}$ (at.%). The calculated mole fraction of equilibrium phases at various temperatures in the $Co_1Cu_1Fe_1Ni_1$ alloy is illustrated in Fig. 8.

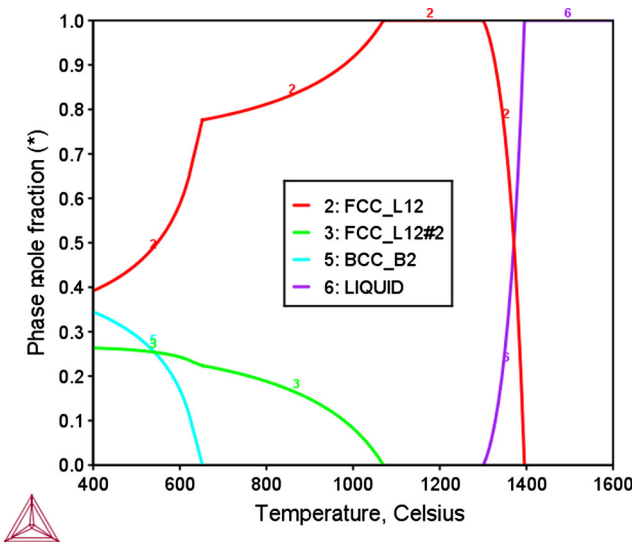

Fig. 8 Calculated mole fraction of equilibrium phases at various temperatures in the CoCuFeNi quaternary alloy with equiatomic ratio

4.3 Transitions from Fcc to Bcc

Relatively the Bcc HEAs have high strength while the Fcc HEAs have good ductility. A proper combination of these two structures in the miscrostructure will result in a superior mechanical property e.g., toughness of the material. It is important to understand the phase stability of Bcc and Fcc varies with the composition. Here we choose Al-containing multi-component systems to exemplify the transition between Bcc and Fcc HEAs and the Bcc + Fcc dual-phase HEAs. Al can be dissolved in many Bcc metals such

as Cr and Fe and form extended solutions. It can even form disordered A2 or ordered B2 solutions with Fcc metals such as Cu and Ni. At the meantime, it shows considerable or large solubilities in Fcc Cu, Fe and Ni. Thus it can be foreseen that adding a small amount of Al to Fcc HEAs may maintain the Fcc structure while a large amount may cause a transformation into the Bcc structure.

$AlxCo_1Cr_1Cu_1Fe_1Ni_1$ is one of the classical HEA systems initially studied by Yeh et al.[1] Surprisingly, no complex intermetallic or intermediates phases formed in as-cast alloys (where $0 \leq x \leq 3.0$ for the mole amount of Al) fabricated by splat quenching at a cooling rate of 10^3-10^4 °C/s. There were only Fcc crystals for alloys for $0 \leq x \leq 0.5$, duplex Fcc + Bcc for $0.8 \leq x \leq 2.5$, and only Bcc for $2.8 \leq x \leq 3.0$. The results were reproduced by Tong et al.[36] through direct solidification into the cold copper hearth. This series of alloys can be considered to be based on $Co_1Cr_1Cu_1Fe_1Ni_1$, as discussed in the previous section 4.1. In the viewpoint of phase diagram, it is the Al addition that promotes the formation of the Bcc phase and its ordered variant (B2). Even though this trend can be predicted based on binary phase diagrams such as Al-Cr and Al-Fe, a direct calculation in the multicomponent system (Fig. 9) is necessary to fully understand the structure transition from Fcc to Bcc with the increase of Al content. The calculation agrees well with experimental results except that the Fcc phase seems slightly underestimated at high Al content ($2.0 \leq x \leq 2.5$).

Considering the V addition, the equiatomic alloy AlCoCrCuFeNiV was studied by Li et al.[37] The XRD pattern revealed the existence of both Bcc and Fcc structures in the as-cast sample. A typical dendrite structure was observed in the SEM image. The EDS results indicated that the interdendritic area is chemically dominated by the Cu element, and the dendritic area has similar concentration for each element but Cu-poor. The phase assemblage of Bcc + Fcc is predicted in Fig. 10 during the solidification process. The primary phase calculated at 1500 °C is a Cu-poor disordered Bcc phase (labeled as BCC_B2 in the figure), which agrees well with the observed dendrites. The Cu-dominating interdendritic area attributes to the disordered Fcc phase (labeled as FCC_L12) which is dominated by Cu according to our calculation. It is interesting to notice that Li et al. also observed some nano-sized precipitates within the dendritic area in the TEM bright image. These particles might be the secondary ordered Bcc phase (i.e., B2 which is labeled as BCC_B2#2 in the figure) precipitates during the fast cooling.

Arc-melt octonary $Al_1Co_1Cr_1Cu_1Fe_1Ni_1Ti_1V_1$ alloys were investigated and the formation of simple crystal structures was reported by Yeh et al.[35] The alloy was either cooled in the cold copper hearth or splat quenched. Both the as-solidified and as-splat-quenched alloys were found to consist of Bcc + Fcc dual phase structure, even though the fraction of Fcc is smaller in the as-splat-quenched alloy. Our calculation (Fig. 11) suggests that there was actually a miscibility gap in the liquid phase and in the Bcc phase. A primary solidification of the disordered Bcc phase (i.e., A2 which is labeled as BCC_B2 in the figure) occurs at 1278 °C in the major liquid, and it is followed by a eutectic solidification of A2 + B2 (labeled as BCC_B2 and BCC_B2#2) between 1198 °C and 1154 °C. A2 is rich in V, Cr and Fe, while B2 is rich in Ti, Co, Ni and Al. Both of them are lean in Cu. The Cu solute is rejected during the

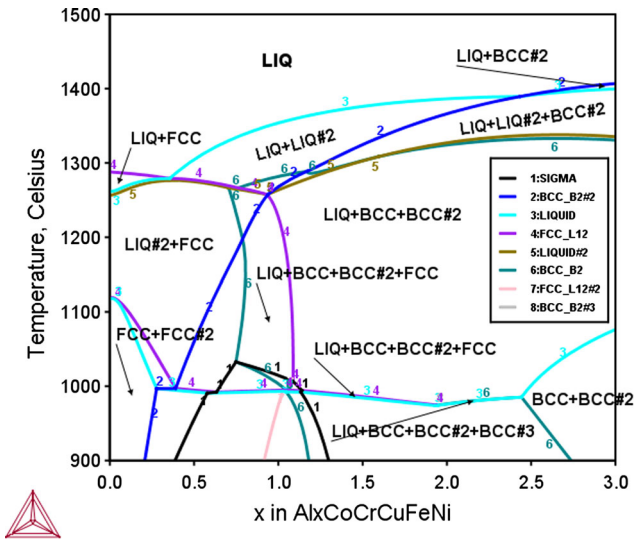

Fig. 9 Predicted phase equilibria in the isopleth for the series of the Al_xCoCrCuFeNi senary alloys, where x = 0-3 represents moles of atoms of the element Al

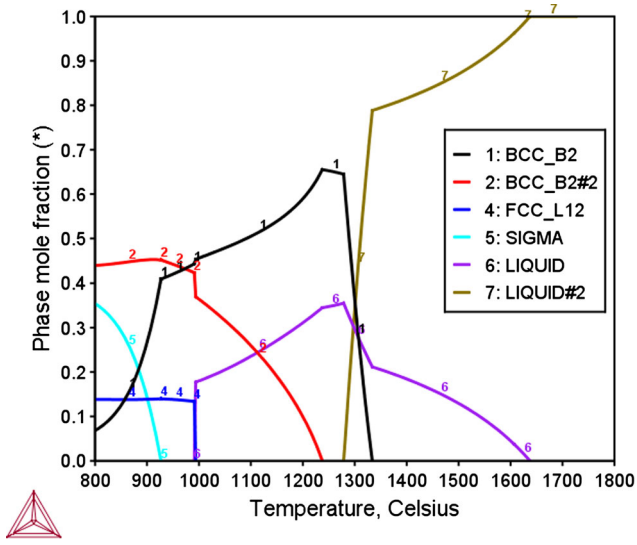

Fig. 10 Calculated mole fraction of equilibrium phases at various temperatures in the AlCoCrCuFeNiV septenary alloy with equiatomic ratio

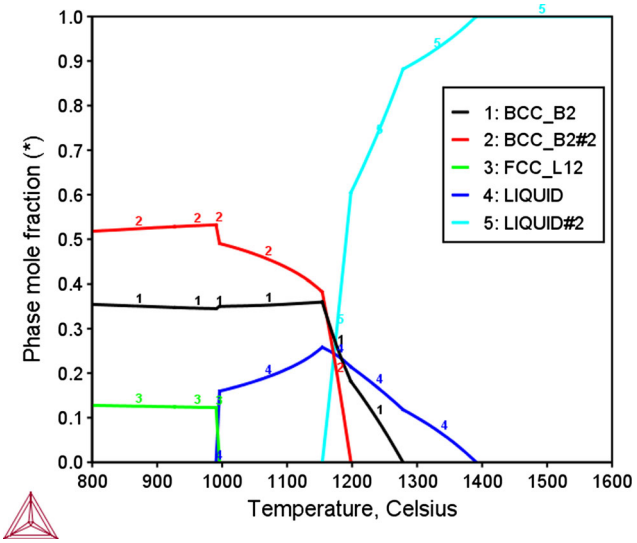

Fig. 11 Calculated mole fraction of equilibrium phases at various temperatures in the AlCoCrCuFeNiTiV octonary alloy with equiatomic ratio

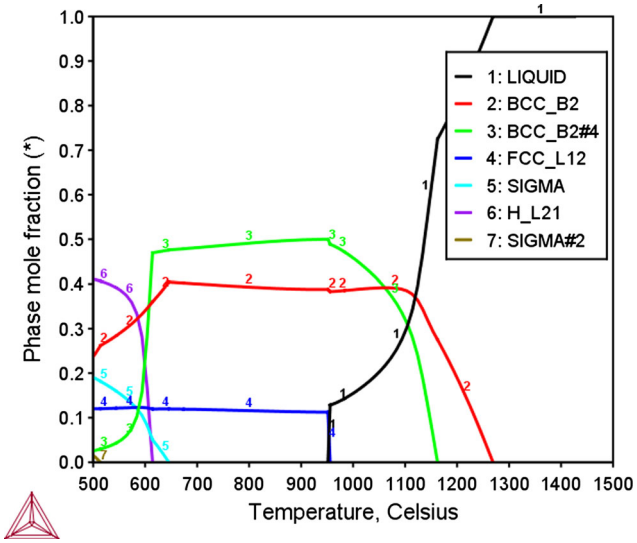

Fig. 12 Calculated mole fraction of equilibrium phases at various temperatures in the AlCoCrCuFeMnNiTiV ennead alloy with equiatomic ratio

solidification of the major liquid (the Curve 5 in Fig. 11) and is accumulated in the other liquid (the Curve 4) whose amount increases during the cooling. This process completes at 1154 °C and then the Cu-rich liquid starts to solidify. The Cu-rich liquid mainly solidifies to the Cu-lean B2 and the constant accumulation of the Cu solute in residual liquid finally causes the formation of Cu-rich Fcc (labeled as FCC_L12 in the figure) at the end of the solidification slightly below 1000 °C. Our calculation not only well accounts for the experimental results, but also provides additional information which had been overlooked in the experimental examinations.

Probably motived by the work of Yeh et al.,[35] Zhou et al.[38] studied the microstructure and compressive properties of the $Al_x(TiVCrMnFeCoNiCu)_{100-x}$ (x = 0, 11.1, 20 and 40) HEAs prepared by inject casting. The alloy at x = 11.1 actually corresponds to the equiatomic composition. The calculated mole fraction of equilibrium phases at various temperatures of this ennead HEA is shown in Fig. 12. It is interesting to notice that the liquid miscibility gap, which appears in the aforementioned octonary alloy, was avoided with the Mn addition. The formation sequence of the solid phases in the ennead alloy, however, is very much similar to that in the octonary alloy. The disordered A2 (labeled as BCC_B2 in the figure) forms first and it was followed by the formation of the eutectic solidification of A2 + B2 (i.e., BCC_B2 and BCC_B2#4 in the figure). Both A2 and B2 are lean in Cu, which agrees well with the observed dendrite composition. The Cu solute was accumulated in the residual liquid, which causes the formation of Cu-rich Fcc (labeled as FCC_L12 in the figure) at the late stage of the solidification. At subsolidus low temperatures even the H_L2_1 phase (the Heusler phase) is predicted being stable.

4.4 Multi-phase Including Intermetallics

Due to the solution hardening multi-component HEAs usually have high strength. It can be further enhanced by the fine precipitation of other phases such as intermetallics from the Bcc or Fcc HEA matrix. Thermodynamic knowledges on the phase equilibria between those phases and HEAs are crucial to design and develop new HEAs. This section illustrates some HEA systems where intermetallic phases such as Laves, sigma, or μ-phase are observed.

The CrNbTiZr equiatomic alloy was studied by Senkov et al.[28] The as-casted samples were further homogenized by annealing at 1200 °C for 24 h, then cooled to room temperature with a cooling rate of 10 °C/min. The microstructure consists of two phases: disordered Bcc and C15_Laves. The Nb- and Ti-enriched regions have a Bcc structure, and the Cr-rich region is Laves. Figure 13 illustrates the mole fraction of equilibrium phases at various temperatures in the CrNbTiZr quaternary alloy. Using TCHEA1 the phase equilibrium at 1473 K gives the following phase compositions: $Cr_{7.6}Nb_{32.7}Ti_{34.6}Zr_{25.1}$ (at.%) in the disordered Bcc (labeled as BCC_B2#2 in the figuire) and $Cr_{66.3}Nb_{6.7}Ti_{2.3}Zr_{24.7}$ (at.%) in C15_Laves.

Adding V into the CrNbTiZr system, Senkov et al.[28] also studied the CrNbTiVZr equiatomic alloy. The microstructure remains consisting of two phases: disordered Bcc and C15_Laves, which is consistent with our calculation on the mole fraction of equilibrium phases at

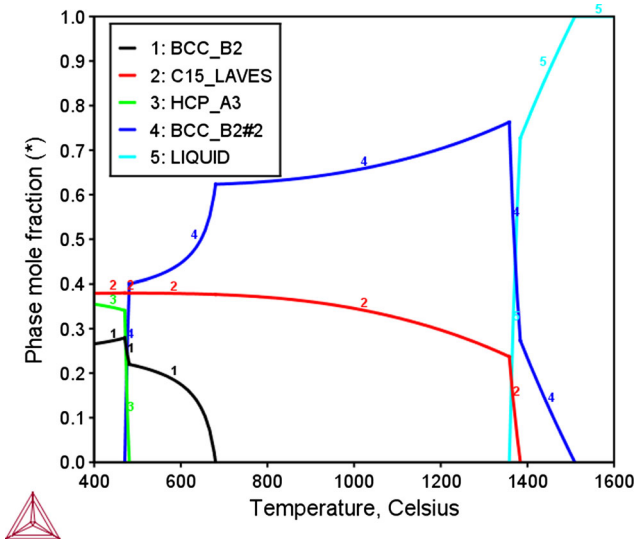

Fig. 13 Calculated mole fraction of equilibrium phases at various temperatures in the CrNbTiZr quaternary alloy with equiatomic ratio

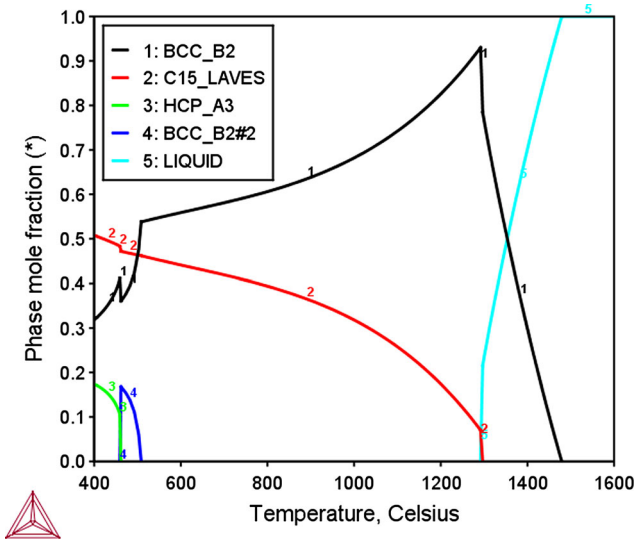

Fig. 14 Calculated mole fraction of equilibrium phases at various temperatures in the CrNbTiVZr quinary alloy with equiatomic ratio

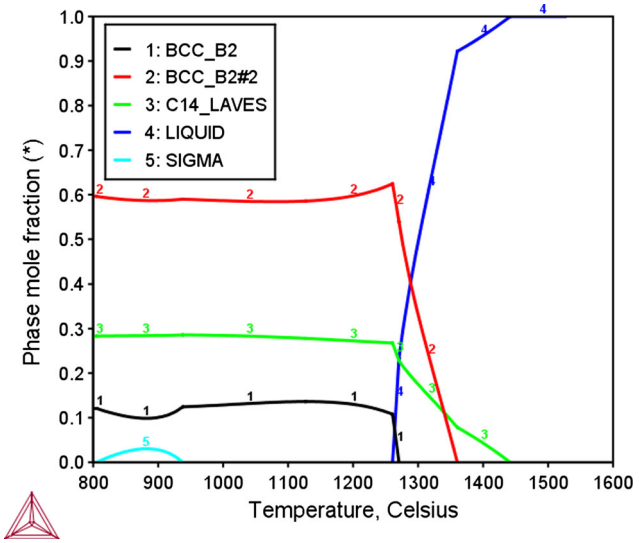

Fig. 15 Calculated mole fraction of equilibrium phases at various temperatures in the $AlCoCrFeNb_{0.5}Ni$ senary alloy

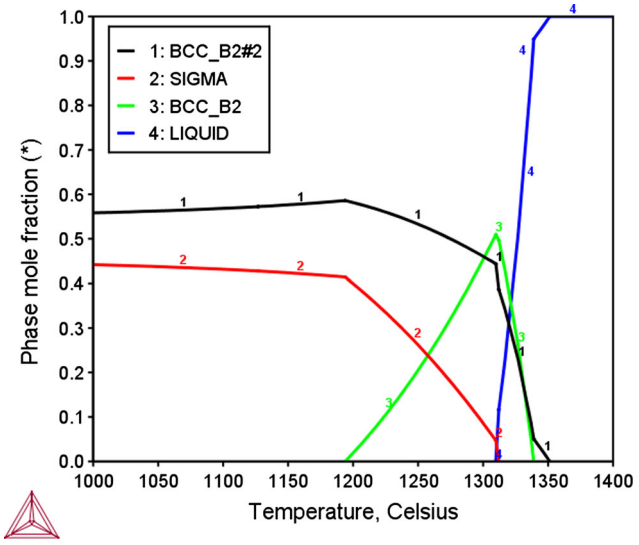

Fig. 16 Calculated mole fraction of equilibrium phases at various temperatures in the $AlCo_{0.5}CrFeMo_{0.5}Ni$ senary alloy

various temperatures in the CrNbTiVZr quinary alloy (Fig. 14). The observed laves phase is enriched with Cr and depleted of Ti, while the Bcc phase (labeled as BCC_B2 in the figure) is rich in both Nb and Ti. Using TCHEA1 such phase compositions are well reproduced for both the Bcc and the C15_Laves phases.

Figure 15 shows the calculated mole fraction of equilibrium phases at various temperatures in the $AlCoCrFeNb_{0.5}Ni$ senary alloy. According to the calculation, both Bcc and C14_Laves phases will form during the solidification. It was verified in the experiments by Ma and Zhang[29] and Zhang et al.[30] Moreover, the observed $(CoCr)_2Nb$ type Laves phase agrees with the predicted C14_Laves in phase composition, e.g., at 1327 °C, $Al_{11.6}Co_{19.6}Cr_{16.6}Fe_{13.5}Nb_{32.0}Ni_{6.7}$ (at.%).

In addition of Bcc phases the sigma phase was also observed in the as-cast $AlCo_{0.5}CrFeMo_{0.5}Ni$ alloy by Hsu et al.[39] and Yeh.[40] Such experimental information verified our calculation on the equilibrium phases at various temperatures (see Fig. 16).

Shun et al.[41] synthesized and analyzed the microstructure and mechanical properties of the $CoCrFeMo_xNi$ quinary alloy series. In the as-cast sample there was a single Fcc for x = 0-0.3, Fcc + sigma for

x = 0.5 and Fcc + sigma + mu for x = 0.85. These phase relations are well reproduced in our calculation (see Fig. 17, FCC_L12 for the disordered Fcc in this case), which demonstrates that TCHEA1 considering all possible phase transformations and equilibria is capable to predict the microstructure of HEA alloys. The chemical compositions of both the sigma and mu phases are predicted as MoCr-rich, in good agreement with the EDS analyses.

The CoFeMnMoNi quinary HEA alloy was investigated by Otto et al.[42] After annealing at 1000 °C for 3 days, a new crystal structure called μ-phase was precipitated from the Fcc matrix. The μ-phase was found being Mo-dominating and Fe- and Co-rich, meanwhile the Fcc phase was Mo-poor. In Fig. 18 one may see that Fcc (labeled as FCC_L12#2) is the only phase in equilibrium with liquid. Below solidus the μ-phase gets stable. At 1000 °C TCHEA1 predicts the two-phase equilibrium of Fcc and μ-phase. The calculated phase composition for the primary Fcc is $Mn_{26.4}Co_{20.1}Mo_{12.2}Ni_{23.2}Fe_{18.2}$ (at.%). For the μ-phase it gives $Mo_{44.4}Fe_{25.7}Co_{19.7}Ni_{10.1}Mn_{0.1}$ (at.%).

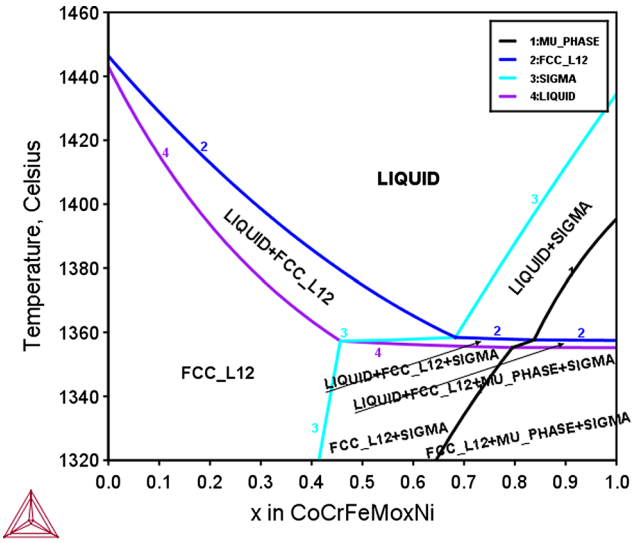

Fig. 17 Predicted phase equilibria in the isopleth for the series of the $CoCrFeMo_xNi$ quinary alloys, where x = 0-1 represents moles of atoms of the element Mo

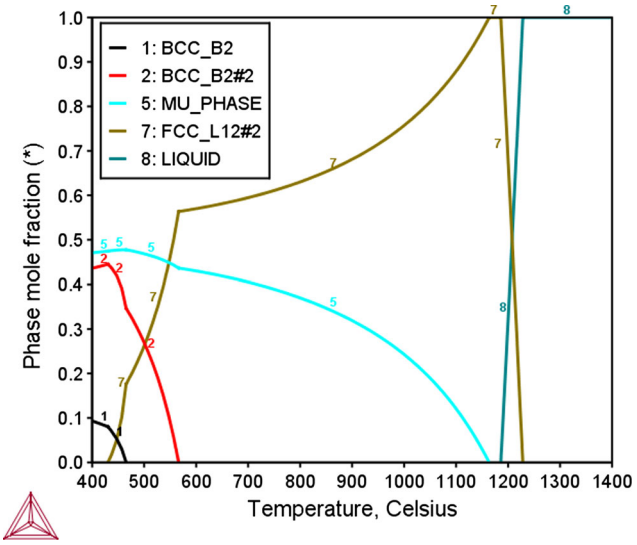

Fig. 18 Calculated mole fraction of equilibrium phases at various temperatures in the CoFeMnMoNi quinary alloy

5 Discussions

The TCHEA1 database is developed based on the CALPHAD approach. It includes almost all possible (stable and metastable) phases. For each phase (no matter stoichiometric or solution) the Gibbs energy is modelled and assessed as a function of temperature and composition. Since the description of the Gibbs energy for all phases is internally consistent, according to the principle of Gibbs energy minimization, thermodynamic equilibrium and corresponding phase diagrams can be reasonably predicted in all sub-systems and in wide temperature ranges. Because TCHEA1 includes most of important elements for Bcc and Fcc HEAs studied so far, moreover, most binary systems and many common ternary systems are thermodynamically assessed critically, TCHEA1 is suitable for the study of phase stability of HEA systems.

The predictability of multi-component CALPHAD database is based on the extrapolation of thermodynamic descriptions from unary, binary and ternary subsystems. The reliability of a database depends on the number and the quality of assessed binary and ternary systems, which are relevant to the alloys that the database focuses on. For a specialized database for HEAs, all the binary and ternary systems may be considered relevant and need to be assessed in principle. The number of ternary systems increases exponentially with the number of components. The assessment of many ternary systems is a daunting challenge that the development of a HEA database faces, as recently pointed out by the present authors.[43] This has never been a problem to the database development for conventional alloys, since about 70 ternary systems containing the principle element might already be sufficient to a database for aluminum or magnesium alloys. All the binary systems and 200 ternary systems have been assessed (over full composition and temperature range for 104 of them) in TCHEA1 within a 15-element small framework. No multi-component Calphad databases have ever achieved such completeness to the best of our knowledge, despite that TCHEA1 covers only about 44% of all 455 ternaries.

It should be clarified that being unassessed does not mean that the description is blank for a ternary system.

Taking the liquid, Bcc, Fcc and Hcp solutions as an example, their energy is described with the model given in Eq 1, consisting of the contributions from lattice stability parameters of pure elements, configuration entropy, binary interaction parameters and ternary interaction parameters. The parameters assessed in all the three unaries and three binaries are used to extrapolate the description of a ternary solution. If necessary, ternary interaction parameters are used and evaluated for accounting for the differences between the extrapolation and the experimental data. Actually, binary interaction parameters are evaluated based on the extrapolation from unaries as well. Binary interactions are fundamental, and ternary ones are important, as all the unary, binary and ternary parameters are to be used for the extrapolation to multi-component compositions. Quaternary and high-order ones are rarely used since their contributions are small and the extrapolation from low-order systems has proved to be reliable in most cases. It is not uncommon that the HEA alloys often consist of elements with similar chemical property, such as the Co-Cr-Fe-Mn-Ni in Fcc HEAs and Nb-Ta-Ti-V-Zr in Bcc HEAs. Naturally the mixing enthalpy among similar elements is small, and the extrapolation is expected to be reasonable even if some ternary interaction parameters are missing. Furthermore, during the development of database, for some ternaries lacking of experimental data the same parameter values are adopted from similar systems, but such ternaries are not counted as assessed in the present paper.

TCHEA1 is developed especially for the high entropy alloys or multi-principle element alloys. It is valid for the composition ranges in the middle of multi-dimensional space, while the compositions corresponding to the corners are taken care of by other individual database for conventional alloys such as Al-, Fe-, or Ni-based. To summarize, TCHEA1 contains many critically assessed ternaries and properly implemented thermodynamic model and model parameters. It aims at the application for HEA systems. The validation of this database against reported HEAs is demonstrated in section 4 of this paper.

It is worth emphasizing that the CALPHAD thermodynamic database dealing with the integral Gibbs energy rather than entropy or enthalpy separately, TCHEA1 gives reliable prediction of phase stability not only for alloys with high entropy, but actually for all alloy systems including the low entropy solutions and other phases such as stoichiometric phases and phase transformations involving ordering and miscibility gap.

Figure 19 shows the calculated mole fraction of equilibrium phases at various temperatures in the CoFeNi alloy which having low configurational entropy since it is a ternary system. It predicts that the primary Fcc phase (labeled as FCC_L12) is stable in a wide temperature range down to 653 °C. The thermal stability of the Fcc phase was confirmed by Singh and Subramaniam[33]: only Fcc was observed in as-cast and as-annealed samples after for 24 h at 850 °C.

Another low entropy alloy, the CrFeNi ternary alloy, was studied by Singh and Subramaniam.[33,44] Using vacuum induction melting they investigated the as-cast CrFeNi alloys which were annealed for 24 h at 950 and 850 °C. According to their XRD pattern there was a single Fcc phase, which agrees well with the formation of the primary Fcc phase (labeled as FCC_L12#2) predicted in Fig. 20. In this Figure it can also be seen that Fcc is stable down to 959 °C, thereafter it decomposes partially into Bcc phase (labeled as BCC_B2#2). In their SEM

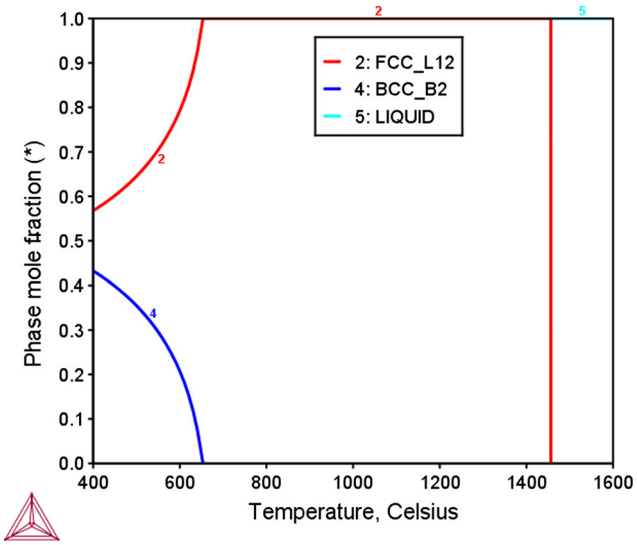

Fig. 19 Calculated mole fraction of equilibrium phases at various temperatures in the CoFeNi ternary alloy

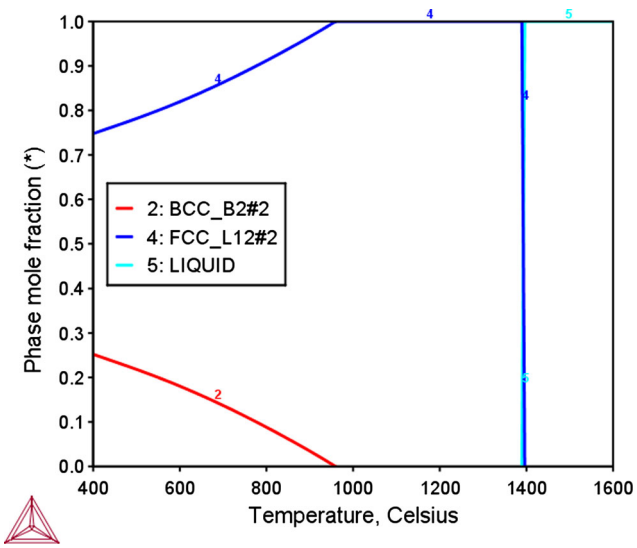

Fig. 20 Calculated mole fraction of equilibrium phases at various temperatures in the CrFeNi ternary alloy with equiatomic ratio

(BSE) images of alloys annealed at the temperatures of either 950 or 850 °C, a small amount of Cr-rich Bcc phase was found along the Fcc grain boundaries. The Bcc phase is believed being precipitated from the Fcc phase during annealing. According to our calculation the major component of this Bcc phase is Cr, which is consistent with the observation.

The configurational entropy reaches maximum for the equiatomic composition in the multi-component systems. Deviating from the center composition the configurational entropy decreases. Chou et al.[45] studied the $Co_{1.5}Cr_1Fe_1Mo_{0.1}Ni_{1.5}Ti_{0.5}$ senary alloy. Even though this composition deviates severely from equiatomic, surprisingly only single Fcc phase was detected in the as-cast sample. The thermal stability of Fcc solution phase relative to all other intermetallic and solution phases was calculated (see Fig. 21). It was predicted that Fcc (labeled as FCC_L12#2) being the primary phase and the only dominating phase in equilibrium with liquid. The predicted Fcc phase being Ti- (and Mo-) poor, agrees well with the experimental information. According to our calculation, at the temperatures slightly above the solidus, minor amount of $Ni_3Ti\_D0_{24}$ phase could precipitate as a secondary phase. The absence of the $Ni_3Ti\_D0_{24}$ phase in the as-cast micro-structure could be a result of small volume fraction below the XRD detection limit for the phase formed during the quenching, or an indication of slight overestimation of such phase stability by the database.

Figure 22 shows the calculated mole fraction of equilibrium phases at various temperatures in the non- equiatomic $Al_{0.3}CoCrFeMo_{0.1}Ni$ senary alloy. The predicted single Fcc phase (labeled as FCC_L12) agrees well the experimental information provided by Shun et al.[46] that only Fcc was observed in the as-cast state.

In addition to the Gibbs energy descriptions, TCHEA1 includes also the volumetric data for all phases. From thermodynamic modeling point of view the volume data is compatible with the Gibbs energy data. By the implementation of proper EOS (Equation of State) which describes the pressure- (or volume-) dependence of Gibbs energy, the TCHEA1 is compatible for the potential extended applications for the high pressure phase stability investigation. Nevertheless, the existing TCHEA1 with the volume data facilitates the estimation of alloy densities. For instance, The Mo-Nb-Ta-W and Mo-Nb-Ta-V-W systems form typical refractory HEAs. Only the single phase Bcc structure was observed in the as-cast sample after repeatedly vacuum arc melting by Senkov et al.[47] The high melting temperature of the MoNbTaVW HEA and the extraordinary thermal stability of the Bcc phase are reproduced in our calculation. Based on TCHEA1 the density of this refractory HEA (i.e., the Bcc phase) is predicted to be 12.35 g/cm^3 at room temperature, which is in excellent agreement with the measured value of 12.36 g/cm^3. More examples for the comparison of measured and calculated HEA density are listed in Table 1.

It has been demonstrated so far in this paper that equilibrium calculations using TCHEA1 can reasonably account for the observed micro-structure in the as-cast and as-annealed alloys. Consider that solidification is a kinetic process, in some cases especially in fast cooling, a Scheil simulation is helpful to understand the solidification behavior. In the Scheil simulation the diffusion in liquid is assumed sufficiently fast while that in solid phases is negligible. Thermodynamic equilibrium reaches locally only at the solid/liquid interface. The liquid composition changes gradually during solidification. Sheikh et al.[48]

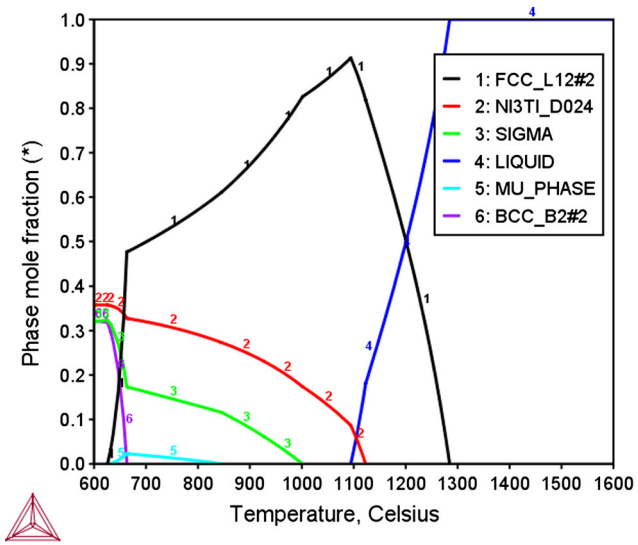

Fig. 21 Calculated mole fraction of equilibrium phases at various temperatures in the $Co_{1.5}CrFeMo_{0.1}Ni_{1.5}Ti_{0.5}$ senary alloy

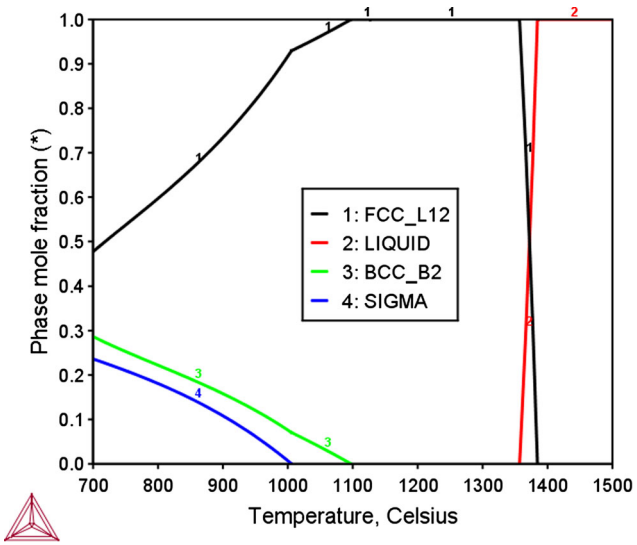

Fig. 22 Calculated mole fraction of equilibrium phases at various temperatures in the $Al_{0.3}CoCrFeMo_{0.1}Ni$ senary alloy

Table 1 Experimental and calculated densities of some HEAs

As-cast HEAs	HfNbTaTiZr	MoNbTaVW	MoNbTaW	AlCrTiV
Phase	Bcc (Bcc)	Bcc (Bcc)	Bcc (Bcc)	B2 (B2)
Exp (Calc)				
Density, g/cm^3	9.94 (9.92)	12.36 (12.35)	13.75 (13.80)	5.06 (5.04)
Exp (Calc)				
References	49	47	47	31

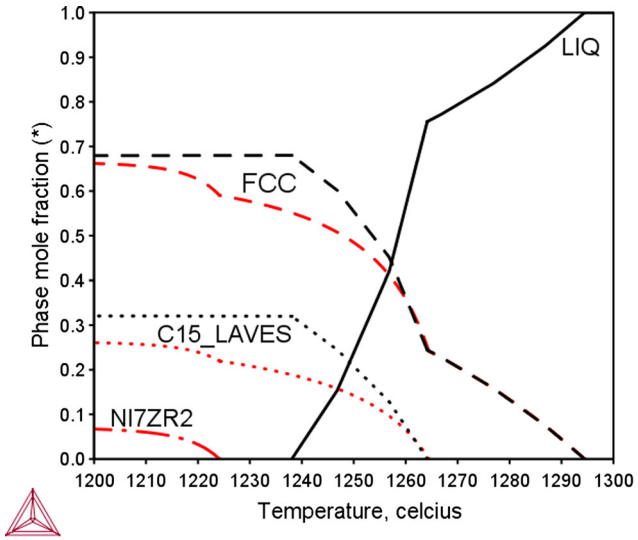

Fig. 23 Predicted solid phase mole fractions by equilibrium (black curves) and Scheil simulation (red curves) of the $CoCrFeNiZr_{0.4}$ alloy (Color figure online)

studied the $CoCrFeNiZr_x$ alloys (x = 0-0.5). In the as-cast $CoCrFeNiZr_{0.4}$ alloy, in addition to the Fcc and C15_Laves phase, minor amount of Ni_7Zr_2 phase was observed. According to the equilibrium calculation, the black curves in Fig. 23, no Ni_7Zr_2 phase was predicted. However, the Scheil simulation, the red curves in Fig. 23, does predicts a minor fraction of solidification of Ni_7Zr_2. One may consider that the global equilibrium calculation and the Scheil simulation mimic two extreme conditions for the solidification process. A real case should happen at the condition in between, depending on the kinetic conditions. To better understand the slow kinetic process, e.g., subsolidus incoherent phase transformations, a mobility database compatible to the thermodynamic database is required to simulate the diffusion controlled phase transformations.

6 Conclusions and Outlook

The TCHEA1 thermodynamic database was developed based on the CALPHAD approach. It includes 15 elements (Al, Co, Cr, Cu, Fe, Hf, Mn, Mo, Nb, Ni, Ta, Ti, V, W and Zr). Within the 15-element framework all the binary systems and many key ternary systems are thermodynamically assessed. According to the validation of TCHEA1 against various HEAs systems up to the ennead (9-element) systems reported in literature, the database predicts reasonably well the phase equilibria in a wide temperature range. Not only has the calculated solidification phase sequence agreed with the observed phase assemblage in microstructures, but also the relative phase amount and composition reached reasonable agreement. The database is suitable but not limited for the study of "high entropy" alloys. The phase equilibrium is determined based on the Gibbs energy minimization, rather than entropy, of the whole system including all possible phases such as solution phases and stoichiometric phases. It is not unusual that in multi-component system there is miscibility gap in the liquid or the primary solid-solution phase at high temperatures close to the solidus. Using TCHEA1 various as-cast and as-annealed micro-structures are reproduced by calculations such as single Bcc or Fcc solutions, dual-phase of Bcc and Fcc, multi-phase including intermetallics of sigma, Laves or μ-phase. Moreover, the predictabilities of phase stability at subsolidus temperatures are demonstrated in the cases of e.g., chemical ordering and miscibility gap of solid solutions at low temperatures. In addition to the Gibbs energy description, the volume data of each phase are also compatibly modeled in TCHEA1, which facilitates the prediction of HEAs' volumetric properties such as density.

In order to better understand the solidification process of HEAs, Scheil simulation could be a supplemental and helpful calculation using TCHEA1. For the process with sluggish kinetics such as incoherent precipitation of other phases from HEA solution phase, one may couple TCHEA1 with a compatible atomic mobility database such as MOBNI4 to study the diffusion controlled solid–solid phase transformations. Combining the thermodynamic and kinetic databases, and applying the "diffusion simulation" module or "precipitation module" available in Thermo-Calc package, one may simulate the nucleation and growth of new phases during such diffusion controlled process.

It was demonstrated in the validation section that TCHEA1 has a reasonable good predictability on the phase equilibria of various HEA systems. However, it does indicate that the stabilities of some phases are overestimated in some cases and underestimated in other cases. The identification of the disagreement between experiments and calculations will

drive the development of TCHEA database series, i.e., to reassess the key parameters of the key phases in the key low-order systems. In addition, in order to extend the application of the database in a wider HEA system more chemical elements need to be included. It's our pleasure to announce that the upgraded version, TCHEA2, is ready to release during the preparation of this manuscript. In the upgraded version the stability of intermetallics such as sigma and Laves phases, and solid solutions of Bcc or Fcc are critically reassessed against the available experimental information in hundreds of HEAs. Moreover, the addition of five new elements (C, N, Re, Ru and Si) extends the application of TCHEA2 database into Hcp HEA, and facilitates the study of equilibria between HEAs and carbides or nitrides or carbonitrides or silicides. It should be reminded that TCHEA is aiming for the application in the middle composition ranges in multi-dimensional space. It is not realistic to assess all the 1140 ternaries in the 20-componenet database. Efforts will be made to estimate more accurately the mixing energy of unassessed ternaries e.g., applying high throughput ab initio calculations. With more and more attentions paid on the HEA subject recently, more extensive (e.g., new systems) and intensive (e.g., atomistic structure) studies are available in literature. A continuous improvement and development of TCHEA database can be expected.

References

1. J.-W. Yeh, S.-K. Chen, S.-J. Lin, J.-Y. Gan, T.-S. Chin, T.-T. Shun, C.-H. Tsau, and S.-Y. Chang, Nanostructured High-Entropy Alloys with Multiple Principal Elements: Novel Alloy Design Concepts and Outcomes, *Adv. Eng. Mater.*, 2004, **6**, p 299-303
2. B. Cantor, I.T.H. Chang, P. Knight, and A.J.B. Vincent, Microstructural Development in Equiatomic Multicomponent Alloys, *Mater. Sci. Eng., A*, 2004, **375-377**, p 213-218
3. M. Tsai and J. Yeh, High-Entropy Alloys: A Critical Review, *Mater. Res. Lett.*, 2014, **2**, p 107-123
4. M.C. Gao, J.W. Yeh, P.K. Liaw, and Y. Zhang, *High-Entropy Alloys, Fundamentals and Applications*, Springer, Cham, 2016
5. D.B. Miracle and O.N. Senkov, A Critical Review of High Entropy Alloys and Related Concepts, *Acta Mater.*, 2017, **122**, p 448-511
6. Y. Zhang, Y.J. Zhou, J.P. Lin, G.L. Chen, and P.K. Liaw, Solid-Solution Phase Formation Rules for Multi-component Alloys, *Adv. Eng. Mater.*, 2008, **10**, p 534-538
7. S. Guo and C.T. Liu, Phase Stability in High Entropy Alloys: Formation of Solid-Solution Phase or Amorphous Phase, *Prog Nat Sci Mater Intl*, 2011, **21**(6), p 433-446
8. C. Zhang, F. Zhang, S. Chen, and W. Cao, Computational Thermodynamics Aided High-Entropy Alloy Design, *JOM*, 2012, **64**, p 839-845
9. A. Manzoni, H. Daoud, S. Mondal, S. van Smaalen, R. Völkl, U. Glatzel, and N. Wanderka, Investigation of Phases in $Al_{23}Co_{15}Cr_{23}Cu_8Fe_{15}Ni_{16}$ and $Al_8Co_{17}Cr_{17}Cu_8Fe_{17}Ni_{33}$ High Entropy Alloys and Comparison with Equilibrium Phases Predicted by Thermo-Calc, *J. Alloys Compd.*, 2013, **552**, p 430-436
10. O.N. Senkov, J.D. Miller, D.B. Miracle, and C. Woodward, Accelerated Exploration of Multi-principal Element Alloys with Solid Solution Phases, *Nature Comm.*, 2015, **6**, p 6529
11. H. Yao, J.-W. Qiao, M.C. Gao, J.A. Hawk, S.-G. Ma, and H. Zhou, MoNbTaV Medium-Entropy Alloy, *Entropy*, 2016, **18**, p 189
12. R. Feng, M.C. Gao, C. Lee, M. Mathes, T. Zuo, S. Chen, J.A. Hawk, Y. Zhang, and P.K. Liaw, Design of Light-Weight High-Entropy Alloys, *Entropy*, 2016, **18**, p 333
13. W.P. Huhn and M. Widom, Prediction of A2 to B2 Phase Transition in the High Entropy Alloy MoNbTaW, *JOM*, 2013, **65**, p 1772-1779
14. F. Tian, L.K. Varga, N. Chen, J. Shen, and L. Vitos, Ab Initio Design of Elastically Isotropic $TiZrNbMoV_x$ High-Entropy Alloys, *J. Alloys Compd.*, 2014, **599**, p 19-25
15. H.L. Lukas, S.G. Fries, and B. Sundman, *Computational Thermodynamics: The Calphad Method*, Cambridge University Press, New York, 2007
16. N. Saunders and A.P. Miodownik, *Calphad—Calculation of Phase Diagrams: A Comprehensive Guide*, Pergamon Press, Oxford, 1998
17. B. Sundman, Thermo-Calc, A General Tool for Phase Diagram Calculations, *Computer Aided Innovation of New Materials*, M. Doyama, T. Suzuki, J. Kihara, and R. Yamamoto, Ed., North Holland, Amsterdam, 1991,
18. J. He, H. Wang, Y. Wu, X. Liu, H. Mao, T. Nieh, and Z. Lu, Precipitation Behavior and its Effects on Tensile Properties of FeCoNiCr High-Entropy Alloys, *Intermetallics*, 2016, **79**, p 41-52
19. D. Choudhuri, B. Gwalani, S. Gorsse, C.V. Mikler, R.V. Ramanujan, M.A. Gibson, and R. Banerjee, Change in the Primary Solidification Phase from Fcc to Bcc-Based B2 in High Entropy or Complex Concentrated Alloys, *Scr. Mater.*, 2017, **127**, p 186-190
20. G. Bracq, M. Laurent-Brocq, L. Perriere, R. Pires, J.-M. Joubert, and I. Guillot, The fcc Solid Solution Stability in the Co-Cr-Fe-Mn-Ni Multi-component, *Acta Mater.*, 2017, **128**, p 327-336
21. T.M. Butler and M.L. Weaver, Investigation of the Phase Stabilities in AlNiCoCrFe High Entropy Alloys, *J. Alloys Compd.*, 2017, **691**, p 119-129
22. A. Takeuchi, T. Wada, and Y. Zhang, MnFeNiCuPt and MnFeNiCuCo High-Entropy Alloys Designed Based on $L1_0$ Structure in Pettifor Map for Binary Compounds, *Intermetallics*, 2017, **82**, p 107-115
23. F. Tancret, I. Toda-Caraballo, E. Menou, and P.E.J.R. Diaz-Del-Castillo, Designing High Entropy Alloys Employing Thermodynamics and Gaussian Process Statistical Analysis, *Mater. Des.*, 2017, **115**, p 486-497
24. I. Ansara, N. Dupin, H.L. Lukas, and B. Sundman, Thermodynamic Assessment of the Al-Ni System, *J. Alloys Comp.*, 1997, **247**(1-2), p 20-30
25. N. Dupin, I. Ansara, and B. Sundman, Thermodynamic Re-Assessment of the Ternary System Al-Cr-Ni, *Calphad*, 2001, **25**(2), p 279-298
26. R. Mathieu, N. Dupin, J.C. Crivello, K. Yaqoob, A. Breidi, J.M. Fiorani, N. David, and J.-M. Joubert, Calphad Description of the Mo-Re System Focused on the Sigma Phase Modeling, *Calphad*, 2013, **43**, p 18-31

27. X. Yang, Y. Zhang, and P.K. Liaw, Microstructure and Compressive Properties of NbTiVTaAl$_x$ High Entropy Alloys, *Procedia. Eng.*, 2012, **36**, p 292-298
28. O.N. Senkov, S.V. Senkova, C. Woodward, and D.B. Miracle, Low-Density, Refractory Multi-principal Element Alloys of the Cr-Nb-Ti-V-Zr System: Microstructure and Phase Analysis, *Acta Mater.*, 2013, **61**, p 1545-1557
29. S.G. Ma and Y. Zhang, Effect of Nb Addition on the Microstructure and Properties of AlCoCrFeNi High-Entropy Alloy, *Mater. Sci. Eng., A*, 2012, **532**, p 480-486
30. Y. Zhang, X. Yang, and P.K. Liaw, Alloy Design and Properties Optimization of High-Entropy Alloys, *JOM*, 2012, **64**, p 830-838
31. Y. Qiu, Y.J. Hu, A. Taylor, M.J. Styles, R.K.W. Marceau, A.V. Ceguerra, M.A. Gibson, Z.K. Liu, H.L. Fraser, and N. Birbilis, A Lightweight Single-Phase AlTiVCr Compositionally Complex Alloy, *Acta Mater.*, 2017, **123**, p 115-124
32. Y.-J. Hsu, W.-C. Chiang, and W. Jiann-Kuo, Corrosion Behavior of FeCoNiCrCu$_x$ High-Entropy Alloys in 3.5% Sodium Chloride Solution, *Mater. Chem. Phys.*, 2005, **92**, p 112-117
33. A.K. Singh and A. Subramaniam, On the Formation of Disordered Solid Solutions in Multi-component Alloys, *J. Alloys Compd.*, 2014, **587**, p 113-119
34. F. He, Z. Wang, Q. Wu, J. Li, J. Wang, and C.T. Liu, Phase Separation of Metastable CoCrFeNi High Entropy Alloy at Intermediate Temperatures, *Scripta Mater.*, 2017, **126**, p 15-19
35. J.-W. Yeh, S.-K. Chen, J.-Y. Gan, S.-J. Lin, T.-S. Chin, T.-T. Shun, C.-H. Tsau, and S.-Y. Chang, Formation of Simple Crystal Structures in Cu-Co-Ni-Cr-Al-Fe-Ti-V Alloys with Multiprincipal Metallic Elements, *Metall. Mater. Trans. A*, 2004, **35**, p 2533-2536
36. C.-J. Tong, Y.-L. Chen, S.-K. Chen, J.-W. Yeh, T.-T. Shun, C.-H. Tsau, S.-J. Lin, and S.-Y. Chang, Microstructure Characterization of Al$_x$CoCrCuFeNi High-Entropy Alloy System with Multiprincipal Elements, *Metall. Mater. Trans. A*, 2005, **36**, p 882-893
37. B.S. Li, Y.P. Wang, M.X. Ren, C. Yang, and H.Z. Fu, Effects of Mn, Ti and V on the Microstructure and Properties of AlCrFeCoNiCu High Entropy Alloy, *Mater. Sci. Eng., A*, 2008, **498**, p 482-486
38. Y.J. Zhou, Y. Zhang, Y.L. Wang, and G.L. Chen, Microstructure and Compressive Properties of Multicomponent Al$_x$(TiVCrMnFeCoNiCu)$_{100-x}$ High-Entropy Alloys, *Mater. Sci. Eng., A*, 2007, **454-455**, p 260-265
39. C.-Y. Hsu, W.-R. Wang, W.-Y. Tang, S.-K. Chen, and J.-W. Yeh, Microstructure and Mechanical Properties of New AlCo$_x$CrFeMo$_{0.5}$Ni High-Entropy Alloys, *Adv. Eng. Mater.*, 2010, **12**, p 44-49
40. J.-W. Yeh, Alloy Design Strategies and Future Trends in High-Entropy Alloys, *JOM*, 2013, **65**, p 1759-1771
41. T.-T. Shun, L.-Y. Chang, and M.-H. Shiu, Microstructure and Mechanical Properties of Multiprincipal Component CoCrFeNiMo$_x$ Alloys, *Mater. Charact.*, 2012, **70**, p 63-67
42. F. Otto, Y. Yang, H. Bei, and E.P. George, Relative Effects of Enthalpy and Entropy on the Phase Stability of Equiatomic High-Entropy Alloys, *Acta Mater.*, 2013, **61**, p 2628-2638
43. H.-L. Chen, H. Mao, and Q. Chen, Database Development and Calphad Calculations for High Entropy Alloys: Challenges, Strategies, and Tips, *Mater. Chem. Phys.* (accepted)
44. A.K. Singh and A. Subramaniam, Thermodynamic Rationalization of the Microstructures of CrFeNi & CuCrFeNi Alloys, *Ad. Mater. Res.*, 2012, **585**, p 3-7
45. Y.L. Chou, J.W. Yeh, and H.C. Shih, The Effect of Molybdenum on the Corrosion Behaviour of the High-Entropy Alloys Co$_{1.5}$CrFeNi$_{1.5}$Ti$_{0.5}$Mo$_x$ in Aqueous Environments, *Corros. Sci.*, 2010, **52**, p 2571-2581
46. T.T. Shun, C.H. Hung, and C.F. Lee, Formation of Ordered/Disordered Nanoparticles in FCC High Entropy Alloys, *J Alloys Comp*, 2010, **493**, p 105-109
47. O.N. Senkov, G.B. Wilks, D.B. Miracle, C.P. Chuang, and P.L. Liaw, Refractory High-Entropy Alloys, *Intermetallics*, 2010, **18**, p 1758-1765
48. S. Sheikh, H. Mao, and S. Guo, Predicting Solid Solubility in CoCrFeNiM$_x$ (M = 4d Transition Metal) High-Entropy Alloys, *J. Appl. Phys.*, 2017, **121**, p 194903
49. O.N. Senkov, J.M. Scotta, S.V. Senkova, D.B. Miracle, and C.F. Woodward, Microstructure and Room Temperature Properties of a High-Entropy TaNbHfZrTi Alloy, *J Alloy Comp*, 2011, **509**, p 6043-6048